Reports

Jupiter's Clouds: Equatorial Plumes and Other Cloud Forms in the Pioneer 10 Images

Abstract. *Pioneer 10 images of Jupiter show bright nuclei in the equatorial zone that appear to be thermally driven sources of cloud plume formations.*

The imaging photopolarimeter experiment aboard the Pioneer 10 spacecraft on its flyby of Jupiter in December 1973 has already been described (*1*); one of the color images from the experiment appeared on the cover of the 25 January 1974 issue of *Science*. The experiment produced two-dimensional maps of intensity and polarization in red and blue light at high spatial resolution. One of the objectives of the experiment was to study the morphology of the Jovian clouds. In this report we describe the cloud forms seen in the equatorial zone and compare them with rotational periods as a function of latitude derived from Earth-based observations of features on Jupiter (*2*).

Figures 1 and 2 are images of Jupiter in blue and red light, respectively, at a subspacecraft resolution of about 800 km. The wide, bright band comprises the southern component of the South Equatorial Belt (SEB_s) and the South Tropical Zone (STrZ), which are separated by a faint, thin, somewhat reddish belt. In general, the belts are darker areas that appear to be brownish or reddish, and the zones are bright and usually mostly white. The Pioneer 10 infrared radiometer observations at 20 and 40 μm (*3*) show relatively low brightness temperatures for this region, which suggests that it is an elevated cloud mass. In Figs. 1 and 2 the SEB_s and STrZ are exceptionally bright and lacking in detail; in other images more features have been present, especially in the SEB_s. We do not know the present rotation period this high in the atmosphere because of the lack of features, but in other years it was close to the radio period of 9 hours 55.5 minutes.

The most striking and new feature seen in Figs. 1 and 2 is the bright, well-defined nucleus in the equatorial zone. A plume appears to be drawn out from the core of this nucleus. Figure 3 shows that there is a swift equatorial jet in this region with a short rotational period. Since the core appears to be the source of the plume, and since it precedes the plume, it appears that the core is in the equatorial jet and that the aerosols which constitute the plume rise to a higher level of the atmosphere with a longer rotational period. Several such plumes have been observed in Pioneer 10 images and can be seen at much lower resolution on Earth-based photographs. The bright cores are usually preceded by festoon-like structures, which appear dark on images taken in the 0.9-μm CH_4 band. These structures

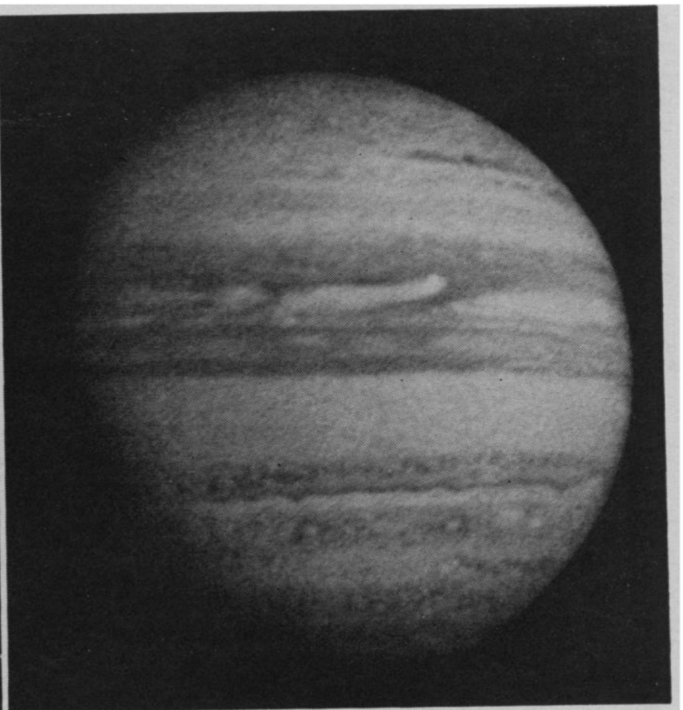

Fig. 1 (left). Blue image of Jupiter from Pioneer 10 received on the earth between 22:17 and 22:46 universal time (U.T.) on 2 December 1973. The spacecraft was 1,840,000 km (~ 26 Jupiter radii) from the center of the planet, and the phase angle (Sun-Jupiter-spacecraft) was 23.5°. North is up and the rising limb is on the left. Fig. 2 (right). As in Fig. 1, but in red light. The fine wavy structures, seen especially in the main bright belt, are not real.

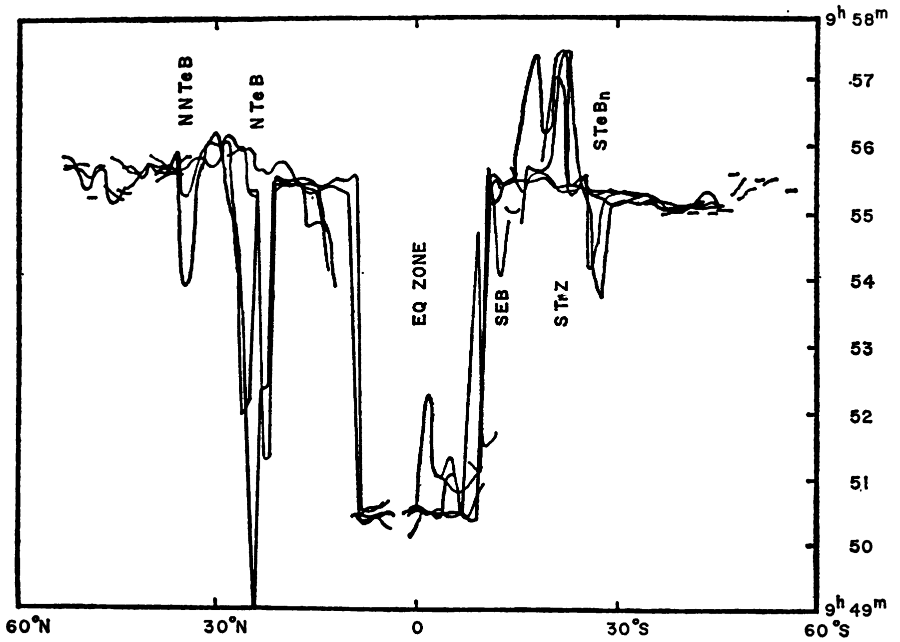

Fig. 3. Rotational period as a function of latitude, as derived from Earth-based observations of spots. This figure is from Chapman (*2*).

have been interpreted as deep gaps in the clouds (*4*) and tend to correlate with 5-μm "hot spots" (*5*).

The plume is drawn out from the nucleus mostly in longitude, but there is also some southward transfer. Such plumes in the Equatorial Zone seem to have their sources near its northern edge. (Northward transfer may occur if the nucleus is in the North Equatorial Belt.) In the north component of the South Equatorial Belt we appear to be looking deep into the atmosphere, as the Pioneer 10 observations at 20 and 40 μm indicate relatively high temperatures there (*3*).

South of the South Tropical Zone is the dark South Temperate Belt (STeB), in which we see, especially in the closer blue pictures such as Fig. 4, elongated cloud forms about 1000 km wide in great curving arcs about 5000 km in diameter. The different rotational rates of the STrZ and the northern component of the South Temperate Belt ($STeB_n$) (see Fig. 3) suggest that shear might contribute to the formation of these features. In the past there have been indications of substantial shear at the boundary between the STeB and the brighter South Temperate Zone (STeZ) below it. This boundary seems wavy with a period of some 5000 km and does not show the arcing structures found in the STeB near the STrZ. Farther south, the STeZ is split by dark, discontinuous filaments, which have occasionally been observed from the earth (*6*, p. 121).

Fig. 4. Closer blue image of a southern part of Jupiter, at the same longitudes as in the right sides of Figs. 1 and 2. The Earth-received times are 17:47 to 19:07 U.T. on 3 December 1973. The spacecraft was about 744,000 km (~10.5 Jupiter radii) from the center of the planet. There still are a few data gaps that will be restored from original records.

South of the STeZ several bright ovals and smaller, light, irregular features appear, surrounded by darker rings (Figs. 1, 2, and 4). The ovals have diameters of several thousand kilometers. The darker rings may be due to removal of condensate from this region through subsiding motion. Features in the South Polar Region are irregular, spotty, and of very low contrast. These are discussed below together with the North Polar Region.

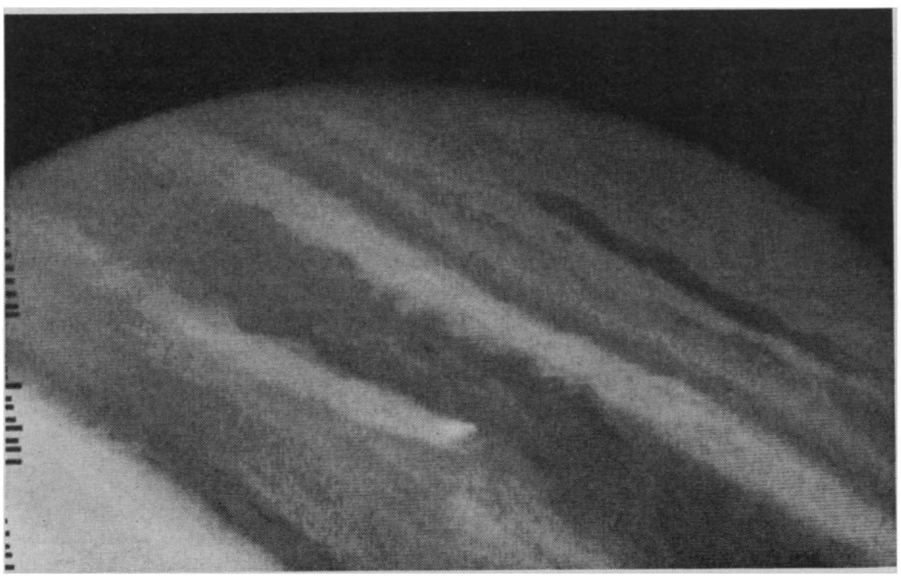

Fig. 5. As in Fig. 4, but of a northern part of Jupiter.

Northward of the dark North Equatorial Belt, the light North Tropical Zone (NTrZ) shows an extensive billowy wave structure and S-shaped swirls curving into the edge of the North Equatorial Belt (NEB). These are shown in a closer view in Fig. 5. The swirls suggest higher zonal clouds veiling part of the NEB. The northern boundary of the NTrZ is well defined by the thin reddish North Temperate Belt (NTeB). While the NTrZ shows detailed features, especially on the southern edge, the NTeB appears rather uniform and so does the North Temperate Zone above it. Figure 3 shows that there is a swift current at the NTeB. The northern North Temperate region shows intricate detail with cell patterns, although these do not appear as marked as in the South Temperate regions.

The North Polar Region begins with a striking, dark, elongated feature (see Figs. 1, 2, and 5). Belts at high latitudes often occur in such discontinuous pieces. Here, some foreshortening must be allowed for because of the southern latitude (−10°) of the subspacecraft point; less than a full hemisphere is observed this close to the planet. Little detail is seen in the North Polar Region. There is a variety of evidence from Earth-based polarimetry (*7*) and photometry (*8*) for greater effective penetration of visible radiation at latitudes higher than about 45° compared with equatorial regions. The deeper penetration of a thick atmosphere appears to be responsible for the relative lack of features in the polar regions.

J. W. Fountain, D. L. Coffeen
L. R. Doose, T. Gehrels
W. Swindell, M. G. Tomasko
University of Arizona, Tucson 85721

References and Notes

1. T. Gehrels *et al., Science* **183**, 318 (1974).
2. C. R. Chapman, *J. Atmos. Sci.* **26**, 986 (1969).
3. S. C. Chase, R. D. Ruiz, G. Münch, G. Neugebauer, M. Schroeder, L. M. Trafton, *Science* **183**, 315 (1974).
4. J. W. Fountain and S. M. Larson, *Lunar Planet. Lab. Commun.* **9**, 315 (1971).
5. C. S. L. Keay, F. J. Low, G. H. Rieke, R. B. Minton, *Astrophys. J.* **183**, 1063 (1973).
6. B. M. Peek, *The Planet Jupiter* (Faber & Faber, London, 1958).
7. T. Gehrels, *Icarus* **10**, 410 (1969).
8. A. E. Clements, thesis, University of Arizona (1974).
9. Supported by the Pioneer Program of NASA/Ames Research Center.

15 March 1974

Variation of P-Wave Velocity before the Bear Valley, California, Earthquake of 24 February 1972

Abstract. *Residuals for* P-*wave traveltimes at a seismograph station near Bear Valley, California, for small, precisely located local earthquakes at distances of 20 to 70 kilometers show a sharp increase of nearly 0.3 second about 2 months before a magnitude 5.0 earthquake that occurred within a few kilometers of the station. This indicates that velocity changes observed elsewhere premonitory to earthquakes, possibly related to dilatancy, occur along the central section of the San Andreas fault system.*

Premonitory changes in seismic-wave velocity in the source regions of earthquakes in the Soviet Union, New York State, the Transverse Ranges of southern California, and Japan have been reported (*1*, *2*). In particular, Wyss and Holcomb (*2*) have shown that observations of teleseismic *P*-wave traveltime residuals (observed minus expected arrival times) at a seismograph station near an approaching shock can be used to detect such changes in velocity. Along the active central section of the San Andreas fault, however, several attempts to observe such changes in *P*-wave velocity have produced generally negative results (*3–5*), and it has been suggested (*6*) that a popular explanation for velocity changes (dilatancy) may not be applicable to strike-slip faults in general.

The Bear Valley earthquake [magnitude (*M*), 5.0] of 24 February 1972 provides an ideal opportunity to search for variations in traveltime residuals for an earthquake along the San Andreas fault, as a U.S. Geological Survey (USGS) seismograph station (BVL) lies nearly above the hypocenter of the event (Fig. 1). Direct application of the method of Wyss and Holcomb, however, is not possible because teleseismic events are poorly recorded at USGS stations that are designed for the detection of small, local events. Moreover, the relatively large errors involved in determining teleseismic residuals require that many separate observations be averaged over long periods of time (*2*). It would be difficult, then, to resolve changes in the traveltime residuals (expected to be less than about 0.4 second) occurring over the 3-month precursor time predicted by the dilatancy model (*7*) for an event with a magnitude of 5.0.

We have made use of abundant local earthquakes to observe *P*-wave traveltime residuals. In particular, we have used small events ($M = 0.7$ to 3.6) located along the Calaveras fault 20 to 70 km northwest of the Bear Valley region during the 1-year period between 1 June 1971 and 30 May 1972. These events (a total of 49 observed sufficiently well at BVL) provide an adequately dense sample in time. And as they can be precisely located, by making use of the network of USGS seismograph stations in the region (*8*), the error in any one observation of the traveltime residual is less than the expected variation due to velocity changes. Figure 1 shows the epicenters of these events and the seismograph stations used to locate them. Each event was located by using only stations within 40 km of the epicenter, and excluding BVL and the nearby stations EKH and JHC (at Elk Horn Ranch and Johnson Canyon), at which we wished to observe traveltime residuals. Under this restriction, all events, large or small, are located with the same station geometry. The location procedure involved adjustments of station delays from those normally used for locating earthquakes throughout central California (*8*) to values more appropriate to the set of earthquakes occurring within this restricted region (*9*). The relative location of events should be significantly improved by this relocation procedure (*10*).

The *P*-wave traveltime residuals so obtained at BVL show a weak dependence on distance from the source, probably due to minor errors in the simplified velocity model for paths from the source region along the Calaveras fault south to the Bear Valley area. This distance trend at BVL was estimated by the relation (determined by least squares)

$$R(\Delta) = 0.300 - 0.0038\Delta$$

where R is the traveltime residual (in seconds) estimated as a function of the distance Δ (in kilometers). Only residuals from the time period preceding the anomaly were used in estimating the distance trend. A correction for the appropriate distance was then removed from each residual. Residuals at JHC and EKH were estimated by the relations

$$\text{(JHC)} \quad R(\Delta) = -0.031 + 0.024\Delta$$

$$\text{(EKH)} \quad R(\Delta) = 1.112 - 0.0341\Delta + 0.00026\Delta^2$$

and were corrected in a similar manner. Alternatively, slightly different velocity models could be used to accomplish the same thing, but three separate models would be necessary. This correction procedure significantly reduces the scatter in the observed residuals (for example, by a factor of ½ at EKH).